

Supporting Information

Mechanisms of Long-Distance Extracellular Electron Transfer of Dissimilatory Metal-reducing Bacterium Mediated by Semiconductive Iron-Oxide Nanominerals

Fumiyoshi Kai¹, Akihiro Okamoto¹, Kazuhito Hashimoto*^{1,2}, and Ryuhei Nakamura*¹

1. Department of Applied Chemistry, School of Engineering, The University of Tokyo, 7-3-1 Hongo, Bunkyo-ku, Tokyo Japan

(*Corresponding Authors' E-mail: hashimoto@light.t.u-tokyo.ac.jp, nakamura@light.t.u-tokyo.ac.jp)

Table of Contents

- 1, XRD analysis (Figure S1)
- 2, TEM analysis (Figure S2)
- 3, Configuration of electrochemical reactor (Figure S3)
- 4, Microbial current generation in the presence of soluble Fe³⁺ ions (Figure S4)
- 5, Linear sweep voltammogram (Figure S5)
- 6, Microbial current generation for *S. oneidensis* MR-1 in the presence of hematite colloids (Figure S6)
- 7, Confocal fluorescence images of the cell-colloidal assembly (Figure S7)
- 8, SEM analysis of the biofilm of delta-2525 mutant (Figure S8)
- 9, Estimation of energy levels of conduction bands for α -Fe₂O₃, α -FeOOH, Fe₃O₄, and γ -Fe₂O₃ (Figure S9)

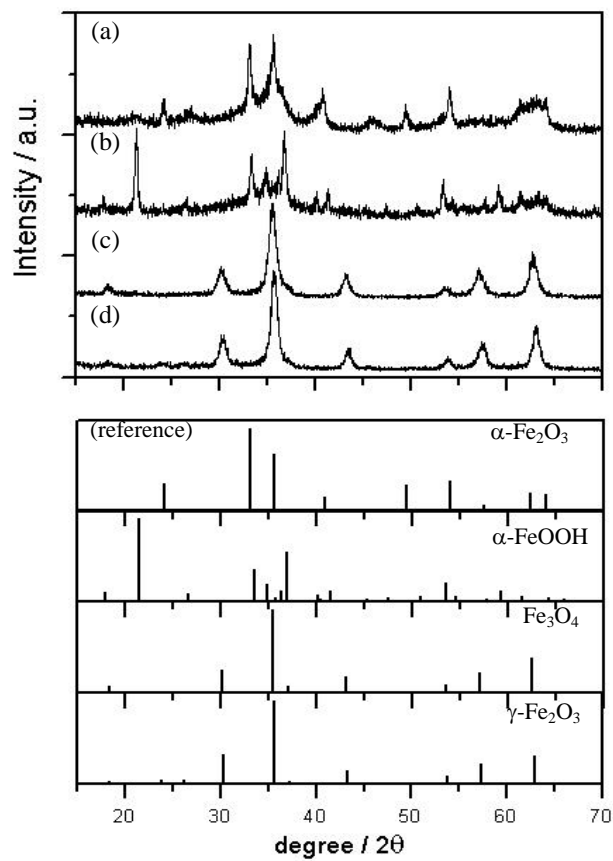


Figure S1. (A) XRD patterns of synthetic iron-oxides colloids (a) α -Fe₂O₃, (b) α -FeOOH, (c) Fe₃O₄, and (d) γ -Fe₂O₃. Each pattern can be assigned to the single phases of α -Fe₂O₃, α -FeOOH, Fe₃O₄, and γ -Fe₂O₃ (Joint Committee on Powder Diffraction Standards (JCPDS) card numbers: 24-0072, 81-0406, 76-1849, and 39-1436, respectively).

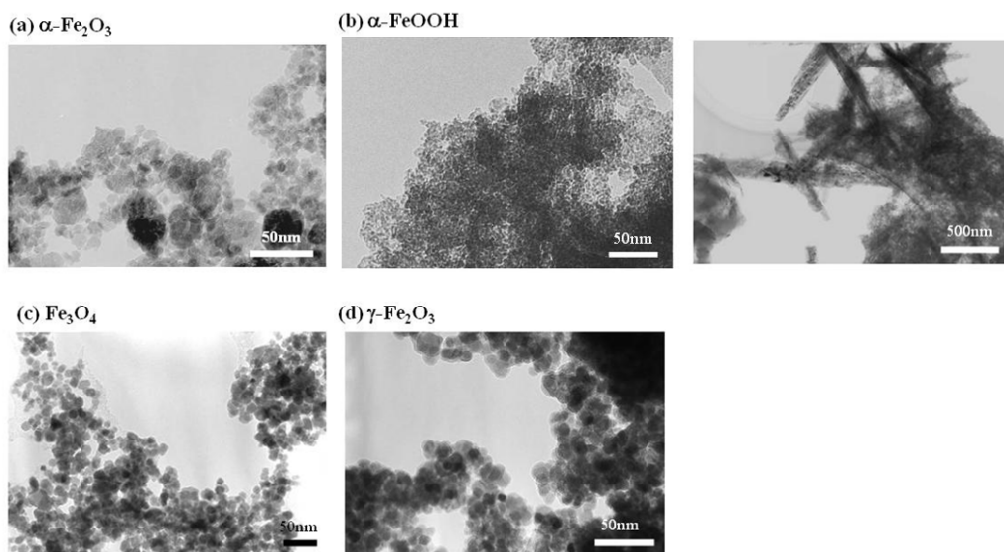


Figure S2. TEM images of synthetic iron-oxides colloids (a) α - Fe_2O_3 , (b and b') α - FeOOH , (c) Fe_3O_4 , and (d) γ - Fe_2O_3 .

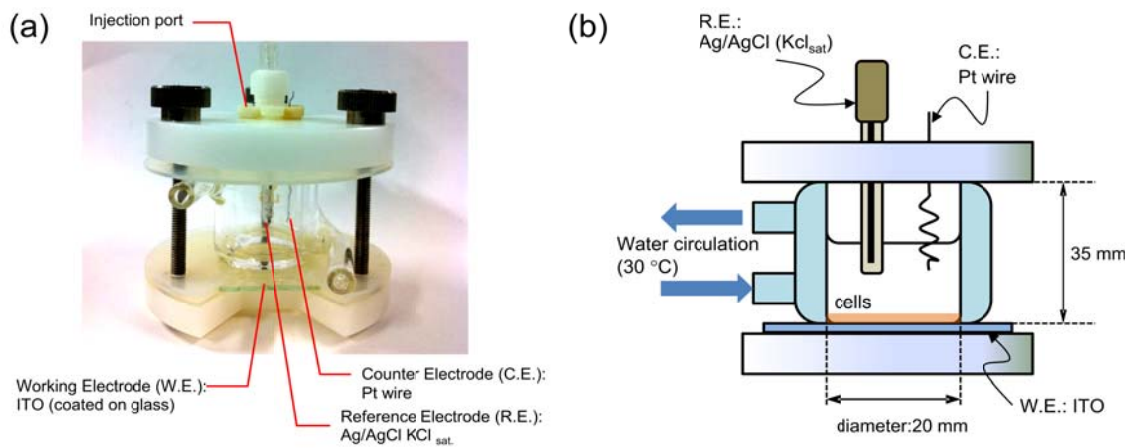


Figure S3. A photograph (a) and schematic illustration (b) of (photo)electrochemical reactor

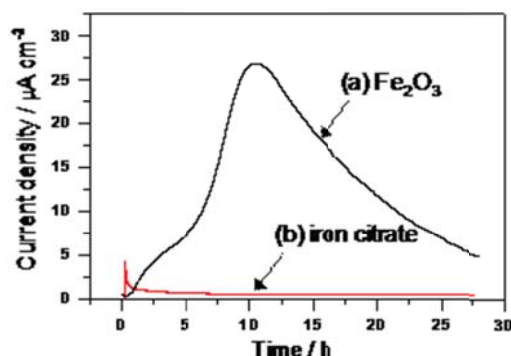


Figure S4. (A) Current (I) vs. time (t) measurements of microbial current generation for *S. loihica* on an ITO glass electrode (a) in the presence of $\alpha\text{-Fe}_2\text{O}_3$ colloids (7.5 mM) and (b) iron citrate (7.5 mM). The temperature of the reactor was maintained at 25 °C. The electrode potential was 0.2 V vs. Ag/AgCl. Note: On the basis of our previous studies (refs *), the electrode potential of ITO was chosen at 0.2 V vs Ag/AgCl, KCl (sat.). This is because electron transfer from ferrous (Fe^{2+}) citrate to ITO becomes a mass-diffusion controlled process at 0.2 V. In other words, the efficiency of electron transfer from ferrous citrate to an electrode no longer has a positive correlation with anodic potential scan.

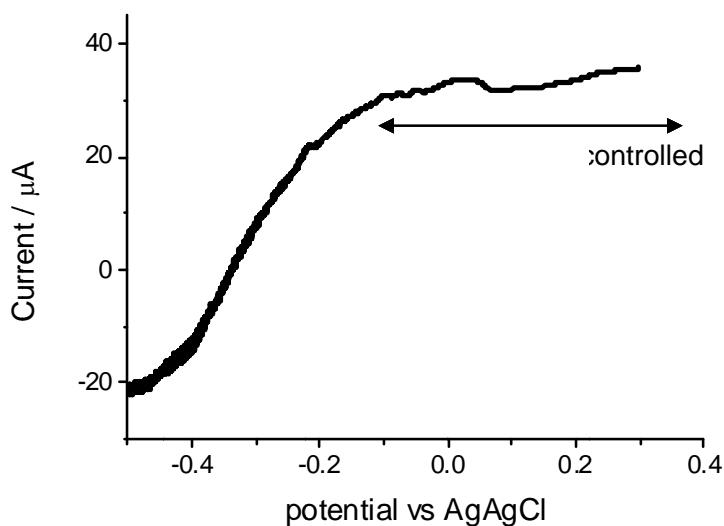


Figure S5. Linear sweep voltammogram for *S. loihica* PV-4 cells inoculated with $\alpha\text{-Fe}_2\text{O}_3$ colloids (7.5 mM).

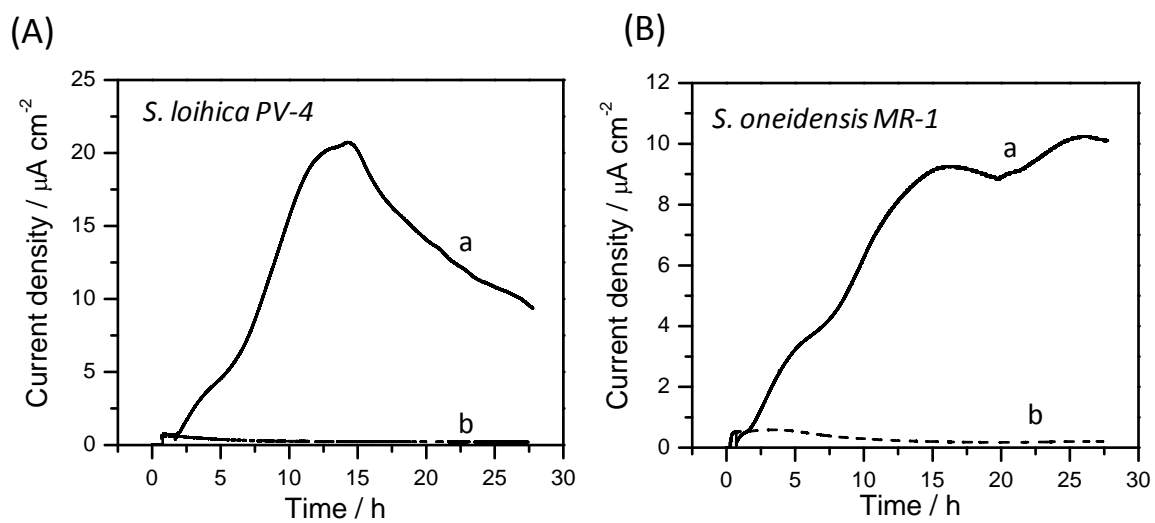


Figure. S6 Microbial current generation of *S. oneidensis* in the (a) presence and (b) absence of $\alpha\text{-Fe}_2\text{O}_3$ colloids (7.5 mM). Density of the cells injected into the reactor was 2.0 of OD_{600} .

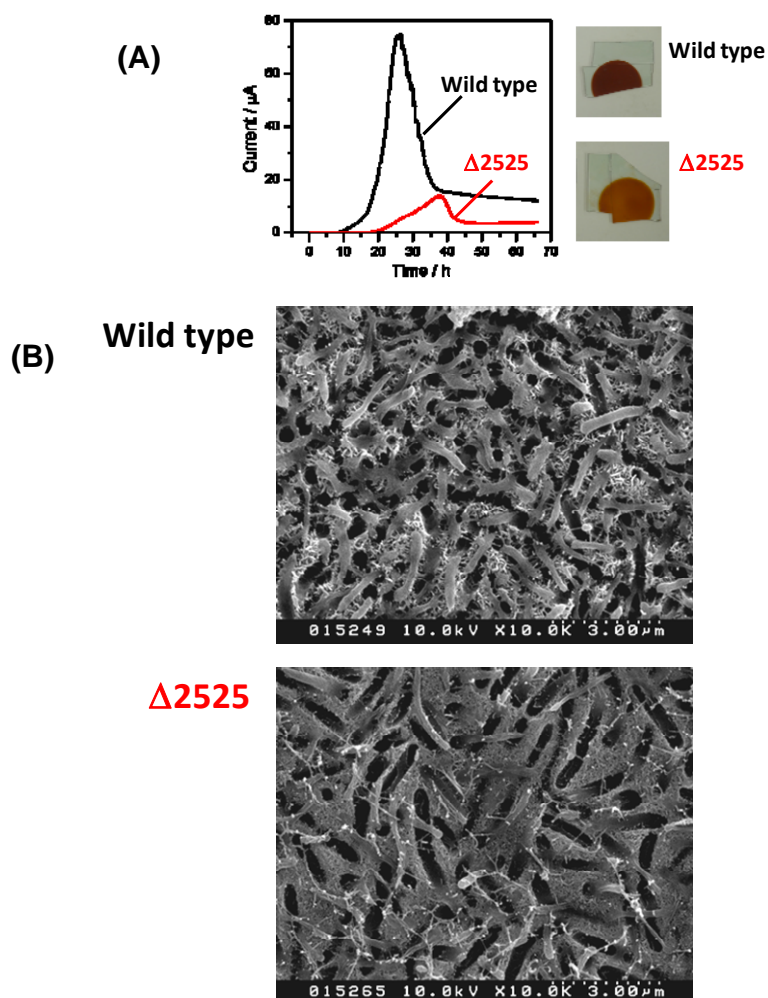


Figure S7. (A) Current density vs. time measurements of current generation by wild-type (WT) cells and $\Delta 2525$ mutant. At $t = 0$, both cell suspension and $\alpha\text{-Fe}_2\text{O}_3$ colloids (7.5 mM) were added into the electrochemical cell. The inserts show the photographs of reactor electrodes obtained at the different stages of current generation for 65 h. (B) SEM images of biofilms obtained for wild cells and $\Delta 2525$ mutant after 65 h of cultivation.

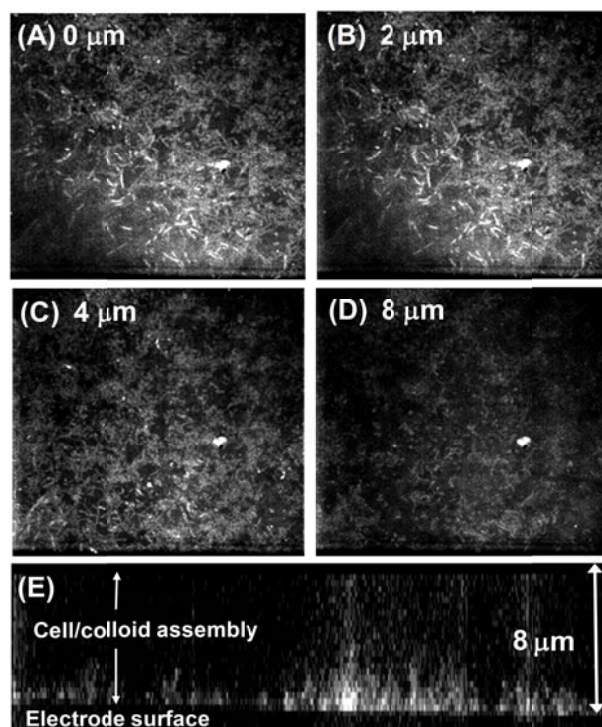


Figure S8 Confocal fluorescence images of the cell-colloidal assemblies grown on the surface of an ITO electrode for 25 h at 0.2 V vs. Ag/AgCl. Panels (A–D) represent *x-y* slices at a distance of 0, 2, 4, and 8 μm from the electrode surface. Panel (E) represents a *z* profile through the structure.

Note: The rod-shaped cells occurred in a high density not only on the electrode surface (panel A), but also at the distance from it. The depth profiles through the cell-colloid film (panel E) showed the existence of the intercellular interaction along the vertical direction, which results in percolation of the cellular network from the electrode to the near surface of the colloidal film.

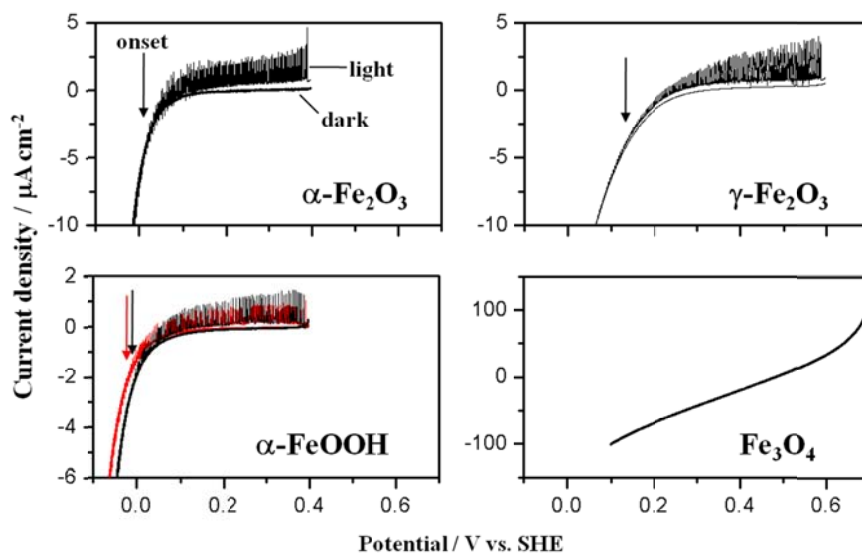


Figure S9. Photocurrent vs potential curves for $\alpha\text{-Fe}_2\text{O}_3$, $\gamma\text{-Fe}_2\text{O}_3$, and $\alpha\text{-FeOOH}$ electrodes. Current vs potential curve for Fe_3O_4 electrode. Deaerated DM-L was used as an electrolyte solution. Scan rate was 4 mV/s.